Epimutations driven by RNAi or heterochromatin evoke antifungal drug resistance in human fungal pathogens

Ye-Eun Son[1] and Joseph Heitman[1*]

[1] *Department of Molecular Genetics and Microbiology, Duke University Medical Center, Durham, NC 27710, USA*

[*] **Corresponding Author:**

213 Research Drive, Durham, NC 27710, USA

Tel: 919-684-2824, Fax: 919-684-2790

Email: heitm001@duke.edu

Keywords: *Mucor*, Epigenetic resistance, RNA silencing, Histone modification, *In vivo* stability

SUMMARY

Antimicrobial resistance is a global health threat emerging through microbe adaptation, driven by genetic variation, genome plasticity or epigenetic regulation. This study investigates how the *Mucor circinelloides* species complex adapts to the antifungal natural product FK506. In *Mucor bainieri*, most resistant strains exhibit unstable phenotypes without genetic changes. Approximately ~50% of FK506-resistant isolates acquire resistance via RNAi-dependent epimutation, where small interfering RNAs (siRNAs) silence *fkbA* transcription. The remaining isolates undergo heterochromatin-mediated silencing via H3K9 methylation and siRNAs spreading, repressing *fkbA* and neighboring genes. One isolate retained only heterochromatin marks without detectable siRNAs. A similar mechanism operates in *Mucor atramentarius*, where FK506 resistance is mediated by ectopic heterochromatin associated with siRNA. Strikingly, heterochromatin-based epimutation inheritance remains stable following *in vivo* infection. These findings reveal that antifungal resistance can arise through distinct, heritable epigenetic pathways involving RNAi, heterochromatin, or both highlighting adaptive strategies employed by ubiquitous eukaryotic microbial pathogens infecting humans.

INTRODUCTION

Fungi are ubiquitous eukaryotic organisms that occupy diverse ecological niches. While many fungi contribute to food production, pharmaceutical development, and biotechnology, others are pathogens capable of infecting a wide range of hosts including humans[1]. The global burden of fungal infections has risen dramatically, now accounting for an estimated two million deaths annually[2,3]. Despite this growing threat, therapeutic options remain limited due to a restricted antifungal arsenal, inadequate diagnostics, and an alarming rise in antifungal resistance. The widespread use of antifungal agents in agriculture and healthcare, combined with environmental pressures such as climate change, has intensified selective pressure on fungal populations, driving the emergence of fungal antimicrobial resistance (fAMR)[4-7].

Fungi employ both genetic and epigenetic strategies to adapt to antifungal stress[8,9]. Genetic changes include point mutations (missense/nonsense) and insertions and deletions (indels) in drug target genes (e.g., *erg11*, *cyp51*, *fks1*), as well as large-scale chromosomal alterations such as copy number variation and aneuploidy. These changes confer resistance in several human fungal pathogens including *Candida albicans*, *Cryptococcus neoformans*, and *Aspergillus fumigatus*[10,11]. In contrast, epigenetic modifications enable non-Mendelian inheritance of resistance without altering the underlying DNA sequence. These include processes such as DNA methylation, RNA interference (RNAi), and ectopic heterochromatin[12].

In *Mucor circinelloides*, RNAi-dependent silencing of *fkbA*—which encodes FKBP12, the cellular target of FK506 (tacrolimus)—confers transient FK506 resistance that reverts in the absence of drug pressure[13]. RNAi-mediated silencing of *pyrF* or *pyrG*

62 prevents conversion of 5-fluoroorotic acid (5-FOA) into its toxic form, leading to transient
63 5-FOA resistance in *Mucor circinelloides*[14]. In addition, heterochromatin-driven gene
64 silencing has been implicated in stress adaptation. In *Schizosaccharomyces pombe*,
65 exposure to caffeine, an environmental stressor, induces the formation of histone 3 lysine
66 9 dimethylation (H3K9me2)-enriched heterochromatin islands that silence genes and
67 promote survival without genetic mutation[15].

68 Mucormycosis is a life-threatening infection caused by Mucorales species
69 including *Mucor* and *Rhizopus*[16]. Spores enter the host via inhalation, traumatic injury, or
70 the rhino-orbital-cerebral route, often resulting in rapid dissemination, especially in
71 immunocompromised individuals with conditions such as diabetes mellitus, malignancy,
72 malnutrition, organ transplantation, or trauma[17,18]. The mortality rate of mucormycosis
73 ranges from 50 to 90%, and incidence surged globally during the COVID-19 pandemic,
74 with over 3,000 deaths reported in India alone[19-21]. Recognizing the severity of
75 mucormycosis, the World Health Organization (WHO) recently designated Mucorales as
76 a high-priority fungal group in the Fungal Priority Pathogens List to drive research and
77 therapeutic development[9,22]. Nonetheless, both intrinsic and acquired antifungal
78 resistance in *Mucor* spp. continue to undermine treatment efficacy, underscoring the
79 urgent need to define resistance mechanisms.

80 The *Mucor circinelloides* complex (MCC) comprises at least 16 phylogenetic
81 species (PS), most of which are predominantly isolated from clinical cases and primarily
82 involved in infections within Mucorales[23]. Prior studies in *M. lusitanicus* and *M.*
83 *circinelloides* have identified both Mendelian and epigenetic mechanisms of FK506
84 resistance, including RNAi-mediated silencing of *fkbA* in the absence of mutations[13,24].

85 However, whether such epigenetic regulation is conserved across other MCC species—
86 or whether alternative mechanisms exist—remains unclear. In this study, we demonstrate
87 that antifungal FK506 resistance in MCC arises through diverse genetic and epigenetic
88 mechanisms, including RNAi-mediated and heterochromatin-mediated silencing. Notably,
89 RNAi and heterochromatin functionally interact to modulate gene expression and confer
90 FK506 resistance in some epimutants. Additionally, we demonstrate that FK506
91 resistance mediated by H3K9me2 heterochromatin is stably inherited after *in vivo*
92 infection, providing new insights into the durability and clinical relevance of epigenetic
93 antifungal resistance.

94 **RESULTS**

95 **Screening of *Mucor circinelloides* species complex (MCC) reveals isolates**
96 **resistant to FK506**

97 Previous studies reported the phylogenetic classification of the MCC and divided
98 the group into 16 phylogenetic species (PS) based on a polyphasic approach that
99 included multi-locus sequence analyses, as well as morphological and physiological
100 characterization[23]. RNAi-mediated epigenetic gene silencing has been shown to play a
101 key role in FK506 resistance in *Mucor lusitanicus* (PS10) and *M. circinelloides* (PS14 and
102 PS15)[13,24]. In this study, we screened multiple species to isolate strains resistant to FK506,
103 a calcineurin inhibitor known to affect the hyphae-to-yeast transition, a process that has
104 been linked to virulence in *Mucor*[25], and rapamycin which inhibits TOR and blocks
105 nutrient-stimulated growth[26]. Following the strategy outlined in **Figure 1A**, spores were
106 collected and point-inoculated on YPD media with or without FK506, and the emergence
107 of resistant colonies was monitored. Resistant colonies were observed in *Mucor janssenii*
108 (PS1), *Mucor bainieri* (PS3), *Mucor atramentarius* (PS6), and *Mucor pseudocircinelloides*
109 (PS13), as well as in the previously reported *M. lusitanicus* (PS10) and *M. circinelloides*
110 (PS14 and PS15) (**Figure S1**).

111 To investigate the underlying mechanisms of resistance, we selected FK506-
112 resistant isolates from *M. janssenii, M. bainieri,* and *M. atramentarius* for further analysis
113 **(Figure 1B)**. The *fkbA* gene, three genes encoding calcineurin catalytic A (*cnaA~C*)
114 subunits, and the calcineurin regulatory B subunit (*cnbR*) gene were amplified and
115 analyzed by Sanger sequencing. As summarized (**Table 1**), four out of ten FK506-
116 resistant isolates from *M. janssenii* exhibited large deletions spanning the *fkbA* locus. An

117 additional five isolates carried large insertions (~4 to 5 kb) in the *fkbA* promoter, nonsense
118 mutations within *fkbA* exons, or point mutations at splice sites. In one isolate, a point
119 mutation in the calcineurin A subunit gene (*cnaA*) was associated with FK506 resistance
120 but retained rapamycin sensitivity. Thus, in *M. janssenii*, all ten isolates exhibited
121 Mendelian mutations. In contrast, analysis of ten FK506-resistant isolates from *M. bainieri*
122 revealed only one isolate with a nonsense mutation in *fkbA*, while the remaining nine
123 exhibited no detectable sequence changes in *fkbA*, or the genes encoding calcineurin A
124 or B subunits, suggesting a possible epigenetic regulation (**Table 1**). Similarly, in *M.*
125 *atramentarius*, among ten FK506-resistant isolates, three harbored nonsense mutations
126 in *fkbA*, one contained a synonymous mutation, two had splice-site point mutations, one
127 had a start-loss mutation, and one had a point mutation in calcineurin B subunit (*cnbR*)
128 (**Table 1**). Notably, two isolates showed no genetic alterations in any of the sequenced
129 genes.
130 These results indicate that all ten FK506-resistant isolates from *M. janssenii* are
131 Mendelian mutants. In *M. bainieri*, one isolate exhibited a Mendelian mutation, while the
132 remaining nine were identified as candidate epimutants. In *M. atramentarius*, eight
133 isolates carried Mendelian mutations, and two were classified as candidate epimutants.
134

135 **FK506-resistant epimutants display reversible phenotypes characterized by**
136 **silenced *fkbA* transcription and FKBP12 protein expression**

137 For FK506-resistant isolates where no DNA sequence alterations were detected
138 in the FK506 target gene *fkbA* or the calcineurin genes, we hypothesized that resistance
139 might be regulated by epigenetic mechanisms. Because epimutations are typically

140 associated with reversible phenotypic plasticity[14], we tested whether FK506 resistance
141 would be lost after successive subculturing on drug-free medium. In fact, FK506
142 resistance was progressively lost following serial passages in the absence of selection
143 pressure (**Figure 2A, 2D; Table 2**). Resistant strains exhibited a hyphal morphology and
144 were capable of sporulation on FK506-containing media, whereas both wild-type (WT)
145 and revertant strains displayed a yeast-like morphology when exposed to FK506
146 treatment (**Figure S2A, S2D**). Additionally, in *M. bainieri*, phenotypic reversion occurred
147 after an average of 15.5 passages, whereas in *M. atramentarius*, reversion required
148 approximately 30 passages (**Figure 2A** and **2D**). Next, considering that epigenetic
149 alterations inhibit target gene expression without changes in the underlying nucleotide
150 sequence, we assayed *fkbA* transcript and FKBP12 protein levels. As shown in **Figure**
151 **2B** and **2E**, the *fkbA* mRNA levels in all FK506-resistant strains were significantly reduced
152 compared to WT and were restored in all reverted strains. Consistently, FKBP12 protein
153 was undetectable in resistant strains and was restored in reverted epimutant isolates
154 (**Figure 2C** and **2F**). These results suggest that drug-resistant strains lacking genetic
155 changes represent epimutants, and that resistance reversion varies both between and
156 within species.
157
158 **Small RNAs confer FK506 resistance in *M. bainieri***
159 To determine which epigenetic mechanisms are involved in FK506 resistance in
160 *M. bainieri*, we first evaluated the potential role of DNA methylation. Whole-genome
161 sequencing data revealed the absence of canonical DNA 5-methylcytosine

162 methyltransferases (DNMT1, DIM-2, RID-1, DNMT4, and DNMT5), consistent with a
163 previous study[27], suggesting that DNA methylation is not involved in FK506 resistance.
164 We next examined the involvement of RNAi by performing sRNA sequencing. As
165 shown in **Figure 3A**, small antisense RNAs mapping to the *fkbA* locus were detected in
166 most FK506-resistant epimutants but were absent in WT and revertant strains. The
167 distribution pattern of sRNAs varied across epimutants: E5–E9 exhibited strong and
168 specific accumulation of sRNAs at the *fkbA* locus. Additional analysis revealed that *fkbA*-
169 targeting sRNAs in E5–E9 averaged approximately 1,000 reads per million (RPM)
170 (**Figure 3B**). The 5′ nucleotide of these sRNAs was predominantly uracil (~82%; **Figure**
171 **3C**), and their length distribution peaked at 21–24 nucleotides (nt) (**Figure 3D**), consistent
172 with the general features of Argonaute-loaded sRNAs[13,28]. These results indicate that E5–
173 E9 epimutants are RNAi-dependent epimutants, in which FK506 resistance is mediated
174 by *fkbA*-targeting antisense sRNAs that silence *fkbA* gene expression.
175 In contrast to E5–E9, which exhibited abundant siRNAs mapping to *fkbA*, isolates
176 E1–E4 lacked detectable *fkbA*-targeting siRNAs (**Figure 3A** and **Figure 3B**). However,
177 E1–E3 displayed siRNAs mapping to neighboring genes (**Figure S3**), with a strong 5′
178 uridine bias and predominant lengths of 21–24 nt. Strikingly, E4 lacked detectable siRNAs
179 at both *fkbA* and its neighboring loci. To determine whether sRNAs spreading at *fkbA*-
180 adjacent loci was associated with transcriptional repression, we performed reverse
181 transcription quantitative PCR (RT-qPCR). As shown in **Figure S3O**, E1–E4 exhibited
182 significant downregulation of genes flanking *fkbA*. However, no significant changes were
183 observed in the expression of *fkbA*-neighboring genes in E7–E9. Meanwhile several

184 genes (e.g., *PS3_009596*, *PS3_009598*) showed significantly altered expression in E5–
185 E6, but these alterations were not associated with sRNA abundance.
186
187 **Heterochromatin marks, along with RNAi, contribute to epigenetic resistance in *M.***
188 ***bainieri***
189 Small RNA spreading has been closely linked to heterochromatin formation and
190 epigenetic gene silencing. Small RNAs targeting specific loci can initiate or reinforce
191 histone modifications, particularly H3K9 methylation [15,29]. To determine whether histone-
192 mediated epigenetic regulation contributes to FK506 resistance in *M. bainieri*, we
193 conducted chromatin immunoprecipitation (ChIP) to assess the abundance of histone H3
194 lysine 9 dimethylation (H3K9me2) in the following epimutants: E1–E3, which exhibit sRNA
195 spreading; E4, which lacks detectable sRNAs but shows transcriptional repression of *fkbA*
196 and neighboring genes; and E8, a canonical RNAi-dependent *fkbA* epimutant. ChIP-
197 qPCR was conducted across the *fkbA* locus, targeting the 5′ UTR, two exonic regions,
198 and the 3′ UTR. H3K9me2 enrichment at the positive control region, which was enriched
199 with small RNAs, was comparable across all strains (**Figure 4A**). H3K9me2 enrichment
200 at *fkbA* locus was negligible in WT, E8, and its revertant E8P28. In contrast, significant
201 enrichment of H3K9me2 was observed in epimutants E1–E4 and was lost upon reversion,
202 suggesting that H3K9me2 is associated with unstable antifungal drug resistance.
203 To further investigate heterochromatin-based epimutational gene silencing, we
204 performed H3K9me2 ChIP-sequencing on the epimutant strains E3, E4, and E8. All
205 strains exhibited similar patterns and levels of H3K9me2 and sRNA at positive control loci,
206 supporting the specificity of the assay (**Figure 4B**). However, in E3 and E4, H3K9me2

207 signals extended beyond the *fkbA* locus into neighboring regions, suggesting
208 heterochromatin spreading (**Figure 4C**). Notably, while E3 showed both H3K9me2 and
209 sRNA spreading, E4 displayed H3K9me2 enrichment without detectable sRNAs. In
210 contrast, the RNAi-dependent epimutant E8 exhibited strong sRNA accumulation
211 specifically at the *fkbA* locus but lacked H3K9me2 enrichment. Taken together, these
212 findings reveal three distinct epigenetic strategies underlying FK506 resistance in *M.*
213 *bainieri* as summarized in **Table 3**: RNAi-associated heterochromatin-dependent
214 mechanisms (Group 1), heterochromatin-dependent only (Group 2), and RNAi-
215 dependent only (Group 3). Interestingly, Group 1 epimutants required fewer passages
216 (average 6.67) for phenotypic reversion compared to epimutants in Group 2 (16.00) or
217 Group 3 (18.80), suggesting that dual-layered epigenetic regulation may promote a more
218 readily reversible resistance state.

219 Next, we sought to determine whether gene silencing in these epimutants is
220 regulated at the pre- or post-transcriptional level. Generally, heterochromatin formation
221 compacts chromatin structure, preventing RNA polymerase II (RNAPII) from accessing
222 DNA and thereby blocking transcription initiation, which is classified as pre-transcriptional
223 regulation[30]. In contrast, RNAi pathways typically involve sRNA that target and degrade
224 transcripts after transcription, representing post-transcriptional regulation[31]. To evaluate
225 the transcriptional status of the *fkbA* locus, we performed RNAPII ChIP-qPCR assays. As
226 shown in **Figure 4D**, RNAPII occupancy at a positive control region, *actA*, was
227 comparable across all strains, while occupancy at the negative control region, which was
228 enriched for sRNAs and marked by H3K9me2, was negligible in all strains. In contrast,
229 the 5′-UTR, exon, and adjacent regions of *fkbA,* where heterochromatin spreading was

230 observed, was significantly reduced in E3 and E4 compared to WT, the RNAi-dependent
231 epimutant E8, and revertant strains. These findings indicate that gene silencing in Group
232 1 (RNAi-associated heterochromatin-dependent mechanisms) and Group 2
233 (heterochromatin-dependent only) occurs at the pre-transcriptional level, whereas
234 silencing in Group 3 (RNAi-dependent only) operates through post-transcriptional
235 regulation.
236
237 **Heterochromatin mediates FK506 resistance in *M. atramentarius***
238 We next assessed whether RNAi- and heterochromatin-based resistance
239 mechanisms identified in *M. bainieri* also operate in *M. atramentarius*, another member
240 of the *Mucor circinelloides* species complex. To evaluate the potential involvement of
241 RNAi, we performed sRNA sequencing. As shown in **Figure 5A**, antisense sRNA
242 spreading was observed across the *fkbA* locus and its flanking regions. Although sRNA
243 abundance at *fkbA* itself was too low (**Figure 5B**), the sRNAs exhibited a strong 5′ uridine
244 bias (**Figure 5C**) and a length distribution peaking at 21–24 nt (**Figure 5D**), consistent
245 with canonical RNAi-derived sRNAs.
246 Given that the pattern of sRNA spreading resembled that observed in
247 heterochromatin-associated epimutants in *M. bainieri* (**Figure S4**), we next examined
248 histone modification. ChIP-qPCR revealed significant H3K9me2 enrichment at the *fkbA*
249 locus in the epimutants (**Figure 5E**). While H3K9me2 enrichment at the positive control
250 locus, which is enriched with small RNAs, was comparable across all strains, expanded
251 H3K9me2 signals at *fkbA* and its neighboring genes, accompanied by sRNA spreading,
252 were strikingly observed exclusively in the epimutant (**Figure 5F** and **5G**). Consistently,

253 RT-qPCR revealed significantly reduced expression of *fkbA*-neighboring genes in the
254 epimutants compared to WT and revertant strains (**Figure S5**). Furthermore, consistent
255 with observations in *M. bainieri*, we observed a significant decrease in RNAPII enrichment
256 at the 5′-UTR, exon, and neighboring regions of *fkbA* in the *M. atramentarius* epimutant,
257 indicating that heterochromatin-mediated gene silencing in *M. atramentarius* is
258 associated with pre-transcriptional regulation (**Figure 5H**). Collectively, these results
259 support the conservation of heterochromatin-mediated FK506 resistance in *M.*
260 *atramentarius*, reinforcing its role as a general epigenetic mechanism across the *Mucor*
261 *circinelloides* complex.
262

263 **Antifungal resistance mediated by heterochromatin is stably inherited following *in***
264 ***vivo* passage**

265 Previous studies reported that RNAi-mediated antifungal resistance can be stably
266 transmitted following *in vivo* passage[32]. To investigate whether heterochromatin-
267 mediated resistance also persists through cell division and stress during host infection,
268 we first examined the maximum growth temperature of *M. bainieri* and *M. atramentarius*.
269 *M. atramentarius* was able to grow at 37 °C, suggesting potential pathogenicity, whereas
270 *M. bainieri* failed to grow under the same condition (**Figure 6A**). To further assess
271 pathogenicity of *M. atramentarius*, we infected fungal spores (1×10^6) via retro-orbital
272 injection in a murine model. Mice infected with *M. circinelloides*, a known pathogen
273 causing mucormycosis, exhibited a significant reduction in survival (**Figure 6B**). Notably,
274 infection with *M. atramentarius* also led to a marked decrease in survival, demonstrating
275 its pathogenic potential.

276 Based on these findings, we infected immunosuppressed mice with equal number
277 of spores from WT, FK506-resistant epimutant (E1), and revertant (E1P32) strains of *M.*
278 *atramentarius*. On day 4 post-infection, brain, liver, spleen, and lung tissues were
279 harvested to assess fungal dissemination. Fungal colonization levels were comparable
280 across strains, with no significant differences observed (**Figure S6A**). Subsequently,
281 when fungal colonies recovered from each organ were tested on FK506-containing media,
282 resistance was retained in colonies derived from epimutant-infected mice (over 80%
283 across organs) in contrast to those derived from WT and revertant strains (**Figure 6C**).
284 Interestingly, a few colonies recovered from the lungs of WT- and revertant-infected mice
285 also exhibited FK506 resistance. Given that heterochromatin mediates FK506 resistance
286 in epimutants, we next asked whether this epigenetic state persists following *in vivo*
287 passage. To address this, we performed ChIP-qPCR on fungal colonies recovered from
288 four organs. FK506-resistant epimutants exhibited robust H3K9me2 enrichment not only
289 at exonic regions but also across the *fkbA* promoter and terminator (**Figure 6D** and
290 **Figure S6B**). By contrast, H3K9me2 levels were minimal or undetectable in WT and
291 revertant strains. These findings indicate that heterochromatin-mediated antifungal
292 resistance is largely stable during host infection, likely maintained through mitotic
293 inheritance of H3K9 methylation marks.

294 **DISCUSSION**

295 Fungal antimicrobial resistance (fAMR) represents an urgent and growing global
296 health threat, jeopardizing human and animal health, agriculture, and food security[7].
297 Although antifungal drugs are widely used to mitigate this burden, the remarkable
298 adaptability of fungi to chemical stressors has rendered them increasingly difficult to
299 control. Paradoxically, dual antifungal therapies intended to improve treatment outcomes
300 may instead accelerate the evolution of multidrug-resistant strains[33-35]. A deeper
301 understanding of the mechanisms driving fAMR is critical for developing effective
302 interventions across clinical and environmental settings.

303 FK506 targets FKBP12, a conserved protein that when bound to FK506 inhibits
304 the calcineurin pathway—an essential regulator of fungal growth, morphogenesis, stress
305 responses, and virulence[36]. In *M. circinelloides*, FK506 enforces a morphological shift
306 from hyphae to yeast-like cells, thereby attenuating pathogenicity[25]. Here, we show that
307 FK506 regulates morphology across the *Mucor circinelloides* complex (**Figure S1**), and
308 that resistance arises via both Mendelian and non-Mendelian mechanisms (**Figure 1**;
309 **Table1**). Our findings expand current models of antifungal resistance by revealing that
310 RNAi- or heterochromatin-mediated epimutations represent alternative, and sometimes
311 independent, pathways. These mechanisms may function separately or synergistically to
312 silence *fkbA*, operating through either post-transcriptional or pre-transcriptional regulation
313 to confer FK506 resistance, and resulting in resistance phenotypes with varying degrees
314 of stability, specificity, and reversibility (**Figure 7**).

315 The interplay between RNAi and histone methylation raises key questions about
316 the sequence and causality of these silencing events. Preexisting heterochromatin can

317 initiate RNAi, as seen in centromeres and transposable elements in *S. pombe* and
318 *Arabidopsis thaliana*, where transcripts from heterochromatic loci are processed into
319 siRNAs that reinforce silencing[37]. In *S. pombe*, chaperone proteins like Hsp90 stabilize
320 the RNA-induced transcriptional silencing (RITS) complex, which recruits Clr4 to nascent
321 transcripts, facilitating heterochromatin formation[38]. Conversely, euchromatic loci may
322 sporadically generate double-stranded RNA, initiating RNAi and leading to
323 heterochromatin deposition via a positive feedback loop[39]. However, in *M. circinelloides*,
324 RNAi and heterochromatin formation have been shown to function independently in
325 repressing transposable elements, contributing to genome stability[27]. Interestingly, in our
326 study, we identified FK506-resistant epimutants with varying combinations of siRNA
327 accumulation and H3K9me2 enrichment at the *fkbA* locus (**Figure 4**). These findings
328 support two non-exclusive models: (1) RNAi-driven initiation of heterochromatin, or (2)
329 heterochromatin-facilitated RNAi. Given that the *fkbA* gene is located in a euchromatic
330 region, the RNAi-first model appears more plausible, although chromatin-initiated RNAi
331 cannot be excluded. Future studies analyzing pathway-specific mutants will be critical to
332 determine the directionality and mechanistic coupling of these epigenetic processes.

333 Maintaining epigenetic silencing is energetically demanding. The RNAi pathway
334 requires ATP for the cleavage of double-stranded RNA by Dicer and the unwinding of
335 siRNA duplexes[40]. Histone methylation also relies on ATP-driven production of S-
336 adenosylmethionine (SAM), a cofactor of histone methyltransferase, and ATP-dependent
337 chromatin remodeling, which is essential for stable heterochromatin maintenance[41,42].
338 These processes reflect a substantial metabolic cost to the cell. Notably, epimutants
339 governed by both RNAi and heterochromatin-dependent silencing exhibited faster

340 phenotypic reversion than those regulated by a single mechanism (**Table 3**). This reduced
341 stability may stem from the cumulative energetic burden of maintaining multiple ATP-
342 intensive pathways. The associated metabolic cost could impose selective pressure
343 favoring reversion, thereby restoring cellular fitness. Alternatively, redundancy or
344 incomplete reinforcement between the two silencing systems may inherently destabilize
345 the dual-layered epimutation, rendering it more prone to reversion than resistance
346 maintained by either pathway alone.

347 Torres-Garcia et al. demonstrated that external stressors such as caffeine induce
348 phenotypic plasticity via Clr4/H3K9me "read-write" systems in *S. pombe*, underscoring
349 the adaptive function of heterochromatin in non-pathogenic fungi[15]. Our findings extend
350 this concept by providing direct evidence that H3K9 methylation contributes to FK506
351 resistance in dimorphic *Mucor* species. Notably, this mechanism operates in pathogenic
352 potential *M. bainieri* and *M. atramentarius* species, suggesting that heterochromatin-
353 mediated resistance is conserved across diverse fungal taxa, spanning both unicellular
354 yeasts and multinuclear hyphal species. While RNAi-dependent antifungal resistance has
355 been shown to be rapidly induced and reversed following *in vivo* passage in a murine
356 model[32], the *in vivo* stability of heterochromatin-dependent epimutants has not been
357 previously characterized. Here, we demonstrate that a heterochromatin-dependent
358 epimutant remains stable *in vivo* (**Figure 6**). The persistence, even in the absence of
359 antifungal pressure, raises the possibility that epigenetically resistant strains could silently
360 disseminate in clinical settings, complicating diagnostics and treatment.

361 In nature, diverse microorganisms, including bacteria, viruses, and fungi, interact
362 continuously, forming complex ecological networks[43-46]. Soil systems are nutrient-rich

363 environments that support a vast diversity of microorganisms, which in turn contribute to
364 essential ecological functions such as nutrient cycling and organic matter decomposition
365 [47,48]. *Streptomyces* is one of the most widely distributed and ecologically significant
366 genera within the phylum Actinobacteria, renowned for its remarkable ability to produce
367 a wide variety of bioactive secondary metabolites, including antifungal compounds[49].
368 Here, we used FK506, a natural antifungal compound that is produced by several
369 *Streptomyces* species, such as *Streptomyces hygroscopicus* and *Streptomyces*
370 *tsukubaensis*[50,51]. Mucorales represent a major fungal order of soil-dwelling saprophytic
371 fungi[52], and thus the ecological coexistence of *Streptomyces* and *Mucor* in soil raises the
372 possibility that natural occurrence of the antifungal natural product FK506 may impose a
373 selective pressure on fungal populations. This pressure may promote the emergence of
374 epigenetic resistance, even in the absence of anthropogenic drug use, by enabling fungi
375 to flexibly modulate gene expression in response to environmental antifungal stress,
376 thereby enhancing their survival and competitive fitness in chemically dynamic
377 ecosystems.

378 In summary, our study extends RNAi-dependent gene silencing to additional
379 *Mucor* species and uncovers that heterochromatin-mediated silencing also drives
380 antifungal resistance. These findings underscore the remarkable epigenetic plasticity of
381 fungal epigenomes and highlight adaptive strategies that enable reversible, yet durable,
382 resistance. Targeting RNAi and chromatin-modifying pathways may thus represent a
383 promising therapeutic strategy against fAMR.

384 **Limitations of the study**

385 This study focused on FK506 resistance under defined *in vitro* and murine *in vivo*
386 conditions within the *M. circinelloides* complex. Whether similar epigenetic mechanisms
387 confer resistance to other antifungal agents or operate in other fungal pathogens remains
388 unknown. Although we propose mechanistic models linking RNAi and heterochromatin,
389 the directionality and mechanistic interdependence of these pathways remain unresolved
390 due to the lack of robust genetic tools in these species. Future studies utilizing pathway-
391 specific mutants will be necessary to dissect these relationships. Moreover, while we
392 demonstrated *in vivo* stability of epimutants, their long-term persistence and impact in
393 chronic infections or alternative host environments warrant further investigation.

394

395 **RESOURCE AVAILABILITY**

396 **Lead contact**

397 Further information and requests for resources should be directed to and will be
398 fulfilled by the lead contact, Joseph Heitman (heitm001@duke.edu).

399 **Materials availability**

400 There are no restrictions on the availability of materials. Strains used in this study
401 are available from the lead contact upon request, or in some case, available from the CBS
402 culture collection.

403

404 **Data and code availability**

405 Whole genome sequencing raw data, genome assembly, small RNA sequencing
406 and ChIP sequencing raw data are available in the NCBI SRA under the project accession
407 numbers PRJNA1242486 (*M. bainieri* CBS293.63) and PRJNA1242487 (*M.*
408 *atramentarius* CBS202.28).

409

410 **ACKNOWLEDGMENTS**

411 We thank Dr. Vikas Yadav for his insightful advice on bioinformatics analyses as
412 well as for his scientific discussions and critical reading. We are grateful to Dr. Carlos
413 Pérez-Arques for his contributions on initial whole genome sequencing, assembly and
414 annotation, as well as for his assistance with *in vivo* training and critical reading, and to
415 Dr. María Isabel Navarro-Mendoza for providing guidance on *in vivo* training. We also
416 thank Anna Floyd Averette for her invaluable support and assistance with *in vivo* assays
417 and Ziyan Xu for preparing DNA for Illumina whole genome sequencing. We appreciate
418 critical reading by Dr. Sheng Sun, Dr. Jun Huang, and Dr. Grit Walther (Hans Knöll
419 Institute). This study was supported by the NIH/National Institute of Allergy and Infectious
420 Diseases (R01 AI170543-03, R01-AI039115-27, and R01-AI050113-20) awarded to J.H..

421 J.H. is co-director and fellow of the CIFAR program Fungal Kingdom: Threats &
422 Opportunities.
423
424 **AUTHOR CONTRIBUTIONS**
425 Conceptualization: Y.S. and J.H.; Methodology: Y.S.; Software: Y.S.; Validation: Y.S.;
426 Investigation: Y.S.; Visualization: Y.S.; Resources: J.H.; Writing – Original Draft: Y.S.;
427 Writing – Review & Editing: Y.S. and J.H.; Supervision: J.H.; Funding Acquisition: J.H.
428
429 **DECLARATION OF INTERESTS**
430 The authors declare no conflicts of interest.
431
432 **STAR METHODS**
433 Detailed methods are provided in the online version of this paper and include the following:
434 **KEY RESOURCES TABLE**
435 **EXPERIMENTAL MODEL AND SUBJECT DETAILS**
436 - Strains, media and growth conditions
437 - Mice
438 - Ethics statement

439 **METHOD DETAILS**
440 - Whole genome sequencing and analysis
441 - Sanger sequencing analysis
442 - RNA extraction and quantitative PCR (qPCR) analysis
443 - sRNA sequencing

444 - Western blot
445 - Chromatin immunoprecipitation (ChIP)-qPCR
446 - ChIP sequencing
447 - *In vivo* infection
448 - Strains recovered after *in vivo* passage

449 **QUANTIFICATION AND STATISTICAL ANALYSES**

450 **SUPPLEMENTAL INFORMATION**

REFERENCES

1. Case, N.T., Gurr, S.J., Fisher, M.C., Blehert, D.S., Boone, C., Casadevall, A., Chowdhary, A., Cuomo, C.A., Currie, C.R., Denning, D.W., et al. (2025). Fungal impacts on Earth's ecosystems. Nature *638*, 49-57. https://doi.org/10.1038/s41586-024-08419-4.
2. McDermott, A. (2022). Drug-resistant fungi on the rise. Proc Natl Acad Sci U S A *119*, e2217948119. https://doi.org/10.1073/pnas.2217948119.
3. Fisher, M.C., and Denning, D.W. (2023). The WHO fungal priority pathogens list as a game-changer. Nat Rev Microbiol *21*, 211-212. https://doi.org/10.1038/s41579-023-00861-x.
4. Lockhart, S.R., Chowdhary, A., and Gold, J.A.W. (2023). The rapid emergence of antifungal-resistant human-pathogenic fungi. Nat Rev Microbiol *21*, 818-832. https://doi.org/10.1038/s41579-023-00960-9.
5. Perlin, D.S., Rautemaa-Richardson, R., and Alastruey-Izquierdo, A. (2017). The global problem of antifungal resistance: prevalence, mechanisms, and management. Lancet Infect Dis *17*, e383-e392. https://doi.org/10.1016/S1473-3099(17)30316-X.
6. Nnadi, N.E., and Carter, D.A. (2021). Climate change and the emergence of fungal pathogens. PLoS Pathog *17*, e1009503. https://doi.org/10.1371/journal.ppat.1009503.
7. Fisher, M.C., Burnett, F., Chandler, C., Gow, N.A.R., Gurr, S., Hart, A., Holmes, A., May, R.C., Quinn, J., Soliman, T., et al. (2024). A one health roadmap towards understanding and mitigating emerging Fungal Antimicrobial Resistance: fAMR. NPJ Antimicrob Resist *2*, 36. https://doi.org/10.1038/s44259-024-00055-2.
8. Lee, Y., Robbins, N., and Cowen, L.E. (2023). Molecular mechanisms governing antifungal drug resistance. NPJ Antimicrob Resist *1*, 5. https://doi.org/10.1038/s44259-023-00007-2.
9. Al Aboud, N.M., Tupper, C., and Jialal, I. (2025). Genetics, Epigenetic Mechanism. In StatPearls. https://www.ncbi.nlm.nih.gov/pubmed/30422591.
10. Flowers, S.A., Colon, B., Whaley, S.G., Schuler, M.A., and Rogers, P.D. (2015). Contribution of clinically derived mutations in *ERG11* to azole resistance in *Candida albicans*. Antimicrob Agents Chemother *59*, 450-460. https://doi.org/10.1128/AAC.03470-14.
11. Lewis, R.E., Liao, G., Hou, J., Prince, R.A., and Kontoyiannis, D.P. (2011). Comparative in vivo dose-dependent activity of caspofungin and anidulafungin against echinocandin-susceptible and -resistant *Aspergillus fumigatus*. J Antimicrob Chemother *66*, 1324-1331. https://doi.org/10.1093/jac/dkr142.
12. Chang, Z., Yadav, V., Lee, S.C., and Heitman, J. (2019). Epigenetic mechanisms of drug resistance in fungi. Fungal Genet Biol *132*, 103253. https://doi.org/10.1016/j.fgb.2019.103253.
13. Calo, S., Shertz-Wall, C., Lee, S.C., Bastidas, R.J., Nicolas, F.E., Granek, J.A., Mieczkowski, P., Torres-Martinez, S., Ruiz-Vazquez, R.M., Cardenas, M.E., and Heitman, J. (2014). Antifungal drug resistance evoked via RNAi-dependent epimutations. Nature *513*, 555-558. https://doi.org/10.1038/nature13575.

14. Chang, Z., Billmyre, R.B., Lee, S.C., and Heitman, J. (2019). Broad antifungal resistance mediated by RNAi-dependent epimutation in the basal human fungal pathogen *Mucor circinelloides*. PLoS Genet *15*, e1007957. https://doi.org/10.1371/journal.pgen.1007957.
15. Torres-Garcia, S., Yaseen, I., Shukla, M., Audergon, P., White, S.A., Pidoux, A.L., and Allshire, R.C. (2020). Epigenetic gene silencing by heterochromatin primes fungal resistance. Nature *585*, 453-458. https://doi.org/10.1038/s41586-020-2706-x.
16. Hernández, J.L., and Buckley, C.J. (2025). Mucormycosis. In StatPearls. https://www.ncbi.nlm.nih.gov/pubmed/31335084.
17. Binder, U., Maurer, E., and Lass-Florl, C. (2014). Mucormycosis--from the pathogens to the disease. Clin Microbiol Infect *20 Suppl 6*, 60-66. https://doi.org/10.1111/1469-0691.12566.
18. Lax, C., Nicolas, F.E., Navarro, E., and Garre, V. (2024). Molecular mechanisms that govern infection and antifungal resistance in Mucorales. Microbiol Mol Biol Rev *88*, e0018822. https://doi.org/10.1128/mmbr.00188-22.
19. Cornely, O.A., Alastruey-Izquierdo, A., Arenz, D., Chen, S.C.A., Dannaoui, E., Hochhegger, B., Hoenigl, M., Jensen, H.E., Lagrou, K., Lewis, R.E., et al. (2019). Global guideline for the diagnosis and management of mucormycosis: an initiative of the European Confederation of Medical Mycology in cooperation with the Mycoses Study Group Education and Research Consortium. Lancet Infect Dis *19*, e405-e421. https://doi.org/10.1016/S1473-3099(19)30312-3.
20. Roden, M.M., Zaoutis, T.E., Buchanan, W.L., Knudsen, T.A., Sarkisova, T.A., Schaufele, R.L., Sein, M., Sein, T., Chiou, C.C., Chu, J.H., et al. (2005). Epidemiology and outcome of zygomycosis: a review of 929 reported cases. Clin Infect Dis *41*, 634-653. https://doi.org/10.1086/432579.
21. Devnath, P., Dhama, K., Tareq, A.M., and Emran, T.B. (2021). Mucormycosis coinfection in the context of global COVID-19 outbreak: A fatal addition to the pandemic spectrum. Int J Surg *92*, 106031. https://doi.org/10.1016/j.ijsu.2021.106031.
22. WHO. (2022). WHO fungal priority pathogens list to guide research, development and public health action https://www.who.int/publications/i/item/9789240060241.
23. Wagner, L., Stielow, J.B., de Hoog, G.S., Bensch, K., Schwartze, V.U., Voigt, K., Alastruey-Izquierdo, A., Kurzai, O., and Walther, G. (2020). A new species concept for the clinically relevant *Mucor circinelloides* complex. Persoonia *44*, 67-97. https://doi.org/10.3767/persoonia.2020.44.03.
24. Perez-Arques, C., Navarro-Mendoza, M.I., Xu, Z., Walther, G., and Heitman, J. (2024). RNAi epimutations conferring antifungal drug resistance are inheritable. bioRxiv. https://doi.org/10.1101/2024.10.15.618540.
25. Lee, S.C., Li, A., Calo, S., and Heitman, J. (2013). Calcineurin plays key roles in the dimorphic transition and virulence of the human pathogenic zygomycete *Mucor circinelloides*. PLoS Pathog *9*, e1003625. https://doi.org/10.1371/journal.ppat.1003625.
26. Bastidas, R.J., Shertz, C.A., Lee, S.C., Heitman, J., and Cardenas, M.E. (2012). Rapamycin exerts antifungal activity in vitro and in vivo against *Mucor*

circinelloides via FKBP12-dependent inhibition of Tor. Eukaryot Cell *11*, 270-281. https://doi.org/10.1128/EC.05284-11.

27. Navarro-Mendoza, M.I., Perez-Arques, C., and Heitman, J. (2023). Heterochromatin and RNAi act independently to ensure genome stability in Mucorales human fungal pathogens. Proc Natl Acad Sci U S A *120*, e2220475120. https://doi.org/10.1073/pnas.2220475120.
28. Mi, S., Cai, T., Hu, Y., Chen, Y., Hodges, E., Ni, F., Wu, L., Li, S., Zhou, H., Long, C., et al. (2008). Sorting of small RNAs into *Arabidopsis* argonaute complexes is directed by the 5' terminal nucleotide. Cell *133*, 116-127. https://doi.org/10.1016/j.cell.2008.02.034.
29. Bhattacharjee, S., Roche, B., and Martienssen, R.A. (2019). RNA-induced initiation of transcriptional silencing (RITS) complex structure and function. RNA Biol *16*, 1133-1146. https://doi.org/10.1080/15476286.2019.1621624.
30. Allshire, R.C., and Madhani, H.D. (2018). Ten principles of heterochromatin formation and function. Nat Rev Mol Cell Biol *19*, 229-244. https://doi.org/10.1038/nrm.2017.119.
31. Filipowicz, W., Jaskiewicz, L., Kolb, F.A., and Pillai, R.S. (2005). Post-transcriptional gene silencing by siRNAs and miRNAs. Curr Opin Struct Biol *15*, 331-341. https://doi.org/10.1016/j.sbi.2005.05.006.
32. Chang, Z., and Heitman, J. (2019). Drug-resistant epimutants exhibit organ-specific stability and induction during murine infections caused by the human fungal pathogen *Mucor circinelloides*. mBio *10*, e02579-02519. https://doi.org/10.1128/mBio.02579-19.
33. Rhodes, J., Abdolrasouli, A., Farrer, R.A., Cuomo, C.A., Aanensen, D.M., Armstrong-James, D., Fisher, M.C., and Schelenz, S. (2018). Genomic epidemiology of the UK outbreak of the emerging human fungal pathogen *Candida auris*. Emerg Microbes Infect *7*, 43. https://doi.org/10.1038/s41426-018-0045-x.
34. Fraaije, B., Atkins, S., Hanley, S., Macdonald, A., and Lucas, J. (2020). The multi-fungicide resistance status of *Aspergillus fumigatus* populations in arable soils and the wider European environment. Front Microbiol *11*, 599233. https://doi.org/10.3389/fmicb.2020.599233.
35. Ikuta, K.S., Mestrovic, T., and Naghavi, M. (2024). Global incidence and mortality of severe fungal disease. Lancet Infect Dis *24*, e268. https://doi.org/10.1016/S1473-3099(24)00102-6.
36. Park, H.S., Lee, S.C., Cardenas, M.E., and Heitman, J. (2019). Calcium-calmodulin-calcineurin signaling: A globally conserved virulence cascade in eukaryotic microbial pathogens. Cell Host Microbe *26*, 453-462. https://doi.org/10.1016/j.chom.2019.08.004.
37. Djupedal, I., and Ekwall, K. (2009). Epigenetics: heterochromatin meets RNAi. Cell Res *19*, 282-295. https://doi.org/10.1038/cr.2009.13.
38. Okazaki, K., Kato, H., Iida, T., Shinmyozu, K., Nakayama, J.I., Murakami, Y., and Urano, T. (2018). RNAi-dependent heterochromatin assembly in fission yeast S*chizosaccharomyces pombe* requires heat-shock molecular chaperones Hsp90 and Mas5. Epigenetics Chromatin *11*, 26. https://doi.org/10.1186/s13072-018-0199-8.

585 39. Yu, R., Wang, X., and Moazed, D. (2018). Epigenetic inheritance mediated by
586 coupling of RNAi and histone H3K9 methylation. Nature *558*, 615-619.
587 https://doi.org/10.1038/s41586-018-0239-3.
588 40. Nykanen, A., Haley, B., and Zamore, P.D. (2001). ATP requirements and small
589 interfering RNA structure in the RNA interference pathway. Cell *107*, 309-321.
590 https://doi.org/10.1016/s0092-8674(01)00547-5.
591 41. Teperino, R., Schoonjans, K., and Auwerx, J. (2010). Histone methyl transferases
592 and demethylases; can they link metabolism and transcription? Cell Metab *12*,
593 321-327. https://doi.org/10.1016/j.cmet.2010.09.004.
594 42. Clapier, C.R., Iwasa, J., Cairns, B.R., and Peterson, C.L. (2017). Mechanisms of
595 action and regulation of ATP-dependent chromatin-remodelling complexes. Nat
596 Rev Mol Cell Biol *18*, 407-422. https://doi.org/10.1038/nrm.2017.26.
597 43. Trivedi, P., Leach, J.E., Tringe, S.G., Sa, T., and Singh, B.K. (2020). Plant-
598 microbiome interactions: from community assembly to plant health. Nat Rev
599 Microbiol *18*, 607-621. https://doi.org/10.1038/s41579-020-0412-1.
600 44. Faust, K., and Raes, J. (2012). Microbial interactions: from networks to models.
601 Nat Rev Microbiol *10*, 538-550. https://doi.org/10.1038/nrmicro2832.
602 45. Weiland-Brauer, N. (2021). Friends or Foes-Microbial Interactions in Nature.
603 Biology (Basel) *10*. https://doi.org/10.3390/biology10060496.
604 46. Getzke, F., Thiergart, T., and Hacquard, S. (2019). Contribution of bacterial-fungal
605 balance to plant and animal health. Curr Opin Microbiol *49*, 66-72.
606 https://doi.org/10.1016/j.mib.2019.10.009.
607 47. de Menezes, A.B., Richardson, A.E., and Thrall, P.H. (2017). Linking fungal-
608 bacterial co-occurrences to soil ecosystem function. Curr Opin Microbiol *37*, 135-
609 141. https://doi.org/10.1016/j.mib.2017.06.006.
610 48. Baumgardner, D.J. (2012). Soil-related bacterial and fungal infections. J Am Board
611 Fam Med *25*, 734-744. https://doi.org/10.3122/jabfm.2012.05.110226.
612 49. Procopio, R.E., Silva, I.R., Martins, M.K., Azevedo, J.L., and Araujo, J.M. (2012).
613 Antibiotics produced by *Streptomyces*. Braz J Infect Dis *16*, 466-471.
614 https://doi.org/10.1016/j.bjid.2012.08.014.
615 50. Kino, T., Hatanaka, H., Hashimoto, M., Nishiyama, M., Goto, T., Okuhara, M.,
616 Kohsaka, M., Aoki, H., and Imanaka, H. (1987). FK-506, a novel
617 immunosuppressant isolated from a *Streptomyces*. I. Fermentation, isolation, and
618 physico-chemical and biological characteristics. J Antibiot (Tokyo) *40*, 1249-1255.
619 https://doi.org/10.7164/antibiotics.40.1249.
620 51. Arndt, C., Cruz, M.C., Cardenas, M.E., and Heitman, J. (1999). Secretion of
621 FK506/FK520 and rapamycin by Streptomyces inhibits the growth of competing
622 *Saccharomyces cerevisiae* and *Cryptococcus neoformans*. Microbiology (Reading)
623 *145 (Pt 8)*, 1989-2000. https://doi.org/10.1099/13500872-145-8-1989.
624 52. Ziaee, A., Zia, M., Bayat, M., and Hashemi, J. (2016). Identification of Mucorales
625 isolates from soil using morphological and molecular methods. Curr Med Mycol *2*,
626 13-19. https://doi.org/10.18869/acadpub.cmm.2.1.13.
627 53. Bushnell, B. (2014). BBMap: A Fast, Accurate, Splice-Aware Aligner.
628 https://sourceforge.net/projects/bbmap/.
629 54. Li, H., Handsaker, B., Wysoker, A., Fennell, T., Ruan, J., Homer, N., Marth, G.,
630 Abecasis, G., Durbin, R., and Genome Project Data Processing, S. (2009). The

631 Sequence Alignment/Map format and SAMtools. Bioinformatics *25*, 2078-2079.
632 https://doi.org/10.1093/bioinformatics/btp352.
633 55. Bolger, A.M., Lohse, M., and Usadel, B. (2014). Trimmomatic: a flexible trimmer
634 for Illumina sequence data. Bioinformatics *30*, 2114-2120.
635 https://doi.org/10.1093/bioinformatics/btu170.
636 56. Langmead, B., and Salzberg, S.L. (2012). Fast gapped-read alignment with Bowtie
637 2. Nat Methods *9*, 357-359. https://doi.org/10.1038/nmeth.1923.
638 57. Zhang, Y., Liu, T., Meyer, C.A., Eeckhoute, J., Johnson, D.S., Bernstein, B.E.,
639 Nusbaum, C., Myers, R.M., Brown, M., Li, W., and Liu, X.S. (2008). Model-based
640 analysis of ChIP-Seq (MACS). Genome Biol *9*, R137. https://doi.org/10.1186/gb-
641 2008-9-9-r137.
642 58. Ramirez, F., Dundar, F., Diehl, S., Gruning, B.A., and Manke, T. (2014). deepTools:
643 a flexible platform for exploring deep-sequencing data. Nucleic Acids Res *42*,
644 W187-191. https://doi.org/10.1093/nar/gku365.
645 59. Son, Y.E., Yu, J.H., and Park, H.S. (2023). The novel spore-specific regulator SscA
646 controls *Aspergillus* conidiogenesis. mBio *14*, e0184023.
647 https://doi.org/10.1128/mbio.01840-23.
648 60. Priest, S.J., Yadav, V., Roth, C., Dahlmann, T.A., Kuck, U., Magwene, P.M., and
649 Heitman, J. (2022). Uncontrolled transposition following RNAi loss causes
650 hypermutation and antifungal drug resistance in clinical isolates of *Cryptococcus*
651 *neoformans*. Nat Microbiol *7*, 1239-1251. https://doi.org/10.1038/s41564-022-
652 01183-z.
653 61. Park, H.S., Man Yu, Y., Lee, M.K., Jae Maeng, P., Chang Kim, S., and Yu, J.H.
654 (2015). Velvet-mediated repression of beta-glucan synthesis in *Aspergillus*
655 *nidulans* spores. Sci Rep *5*, 10199. https://doi.org/10.1038/srep10199.
656 62. Navarro-Mendoza, M.I., Perez-Arques, C., Panchal, S., Nicolas, F.E., Mondo, S.J.,
657 Ganguly, P., Pangilinan, J., Grigoriev, I.V., Heitman, J., Sanyal, K., and Garre, V.
658 (2019). Early diverging fungus *Mucor circinelloides* lacks centromeric histone
659 CENP-A and displays a mosaic of point and regional centromeres. Curr Biol *29*,
660 3791-3802 e3796. https://doi.org/10.1016/j.cub.2019.09.024.
661 63. Robinson, J.T., Thorvaldsdottir, H., Turner, D., and Mesirov, J.P. (2023). igv.js: an
662 embeddable JavaScript implementation of the Integrative Genomics Viewer (IGV).
663 Bioinformatics *39*. https://doi.org/10.1093/bioinformatics/btac830.
664

665 **STAR METHODS**

666 **KEY RESOURCES TABLE**

REAGENT or RESOURCE	SOURCE	IDENTIFIER
Antibodies		
FKBP12 Polyclonal Antibody	Invitrogen	Cat# PA1-026A
GAPDH Polyclonal antibody	Proteintech	Cat# 10494-1-AP
Anti-Histone H3 (di methyl K9) antibody	Abcam	Cat# ab1220
Anti RNA pol II antibody	Active Motif	Cat# 39097
Chemicals and Proteins		
yeast extract peptone dextrose	BD Bioscience	Cat# 242710
Tacrolimus	Astellas Pharma	Cat# NDC 0469-3016-01
Rapamycin	API Chem	Cat# AC-722
Tissue & Cell Lysis Buffer	Lucigen	Cat# MTC096H
MPC Protein Precipitation Reagent	Lucigen	Cat# MMP095H
Maxima H Minus cDNA Synthesis Master Mix with dsDNase	ThermoFisher	Cat# M1681
PowerUp SYBR Green Master Mix	ThermoFisher	Cat# A25780
Pierce RIPA buffer	ThermoFisher	Cat# 89901
Protease inhibitor tablet	Roche	Cat# 4693132001
Novex Tris-Glycine SDS Sample Buffer	Invitrogen	Cat# LC2676
PageRuler Prestained Protein Ladder, 10 to 180 kDa	ThermoFisher	Cat# 26616
Novex Tris-Glycine Mini Protein Gels, 16%, 1.0 mm	Invitrogen	Cat# XP00162BOX
16% Formaldehyde	ThermoFisher	Cat# 28908
Glycine	Sigma-Aldrich	Cat# G7126
HEPES, 1.0 M buffer, pH 7.5	ThermoFisher	Cat# J60712.AP
Sodium chloride	ThermoFisher	Cat# S271-500
EDTA (0.5 M), pH 8.0, RNase-free	ThermoFisher	Cat# AM9261
Triton X-100	Sigma-Aldrich	Cat# T9284
Sodium deoxycholate	Sigma-Aldrich	Cat# 30970
Dynabeads Protein A/G	Invitrogen	Cat# 80105G
Cyclophosphamide	Sigma-Aldrich	Cat# C7397-1G
Critical commercial assays		
Fungi/Yeast Genomic DNA Isolation Kit	Norgen Biotek	Cat# 27300
miRNeasy Mini Kit	Qiagen	Cat# 217004
miRNA Library Kit	Qiagen	Cat# 331502

Pierce BCA Protein Assay Kit	ThermoFisher	Cat# 23227
MAGnify™ Chromatin Immunoprecipitation System	Invitrogen	Cat# 492024
KAPA HyperPrep	Roche	Cat# 07962355001
Deposited data		
Whole genome sequence data	This paper	PRJNA1242486, *M. bainieri*; PRJNA1242480, *M. atramentarius*
sRNA sequence data	This paper	PRJNA1242486, *M. bainieri*; PRJNA1242480, *M. atramentarius*
ChIP sequence data	This paper	PRJNA1242486, *M. bainieri*; PRJNA1242480, *M. atramentarius*
Experimental models: Organisms/strains		
Mouse: BALB/cAnNCrl	Charles River Laboratories	Strain code 028
Mucor circinelloides complex	[23]	N/A
FK506-resistant *Mucor* strains	This paper	See **Table S2**
Oligonucleotides		
Primer for PCR and qPCR	This paper	See **Table S1**
Software and algorithms		
BBDuk	[53]	https://github.com/BioInfoTools/BBMap
BBMap	[53]	https://github.com/BioInfoTools/BBMap
SAMtools v1.21	[54]	https://github.com/samtools/samtools
IGV v2.16.0	Integrative Genome Viewer	https://igv.org/
Trimmomatic v0.39	[55]	https://github.com/usadellab/Trimmomatic
Bowtie2 v2.5.4	[56]	https://github.com/BenLangmead/bowtie2
MACS3 v3.0.3	[57]	https://github.com/macs3-project/MACS
BamCoverage v3.5.6	[58]	https://github.com/deeptools/deepTools
GraphPad Prism v10.1.1	GraphPad Software	https://www.graphpad.com/updates/prism-10-1-1-release-notes
R v4.3.2	R-Studio	https://www.r-studio.com/
Other		
T100 Thermal Cycler	Bio-Rad	https://www.bio-rad.com/en-us/sku/1861096-t100-thermal-cycler?ID=1861096

FastPrep bead-beater	MP Biomedicals	https://www.mpbio.com/us/fastprep-24-classic-instrument-1-each
Zirconia-silica beads	BioSpec Products	Cat# 11079105z
QuantStudio 3 qPCR system	ThermoFisher	https://www.thermofisher.com/order/catalog/product/A28567
NovaSeq X platform	Illumina	https://www.illumina.com/systems/sequencing-platforms/novaseq-x-plus.html
ChemiDoc MP imaging system	Bio-Rad	https://www.bio-rad.com/en-us/sku/12003154-chemidoc-mp-imaging-system?ID=12003154
Bioruptor Plus sonication device	Diagenode	https://www.diagenode.com/en/p/bioruptor-plus-sonication-device

667

668 **EXPERIMENTAL MODEL AND SUBJECT DETAILS**

669 **Fungal strains, media and growth conditions**

670 *Mucor* strains studied here are described in **Table S1**. *Mucor* strains were grown
671 on liquid or solid yeast extract peptone dextrose (YPD; BD, Difco, Franklin Lakes, NJ,
672 USA) at room temperature. To isolate FK506-/rapamycin-resistant strains, 10^5 spores
673 were inoculated onto solid YPD, supplemented with antifungal drug 1 μg/mL of FK506
674 (Astellas Pharma, Chuo, Tokyo, Japan) and 100 ng/ml of rapamycin (API Chem,
675 Hangzhou, Zhejiang, Chian) and incubated for 3, 5, 7 days[13]. To test the stability of
676 FK506-resistant strains, spores of the resistant strains were collected and inoculated in
677 liquid YPD without any drugs overnight[14]. After several rounds of subculturing, the
678 passaged cells were spotted onto YPD or YPD with FK506 to confirm phenotypic plasticity.
679

680 **Mice**

681 Male BALB/cAnNCrl mice, 6 to 7 weeks old, were obtained from Charles River
682 laboratory (Wilmington, MA, USA). Mice were maintained in a pathogen free animal
683 facility and anesthetized with isoflurane before infection.
684

685 **Ethics statement**

686 All animal experiments in this study were approved by the Duke University
687 Institutional Animal Care and Use Committee (IACUC) (protocol #A224-23-11). Animal
688 care and experiments were conducted according to IACUC ethical guidelines.

689 **METHOD DETAILS**

690 **Whole genome sequencing and analysis**

691 For short-read sequencing, *Mucor* strains were cultured on YPD medium for three
692 days, then collected and lyophilized. After breaking the cells, genomic DNA (gDNA) was
693 extracted with the Fungi/Yeast Genomic DNA Isolation Kit (Norgen Biotek, Thorold,
694 Ontario, Canada). gDNA libraries were constructed with the Kapa HyperPlus library kit
695 (Roche, Basel, Switzerland) and paired end reads were sequenced on an NovaSeq X
696 platform (Illumina, San Diego, CA, USA).

697

698 **Sanger sequencing analysis**

699 *Mucor* strains were cultured on YPD medium for three days and gDNA was
700 extracted from with the Tissue & Cell Lysis Buffer (Lucigen, Middleton, WI, USA) and
701 MPC Protein Precipitation Reagent (Lucigen). The promoter, open reading frame, and
702 terminator regions of the *fkbA* gene were amplified by polymerase chain reaction (PCR)
703 using primers listed in **Table S2**. The purified PCR products were sequenced and
704 analyzed against the reference *fkbA* sequence.

705

706 **RNA extraction and quantitative PCR (qPCR) analysis**

707 Total RNA was extracted from Mucor cells cultured on YPD, with or without FK506,
708 at room temperature. After overnight lyophilization, each sample was homogenized in a
709 FastPrep bead-beater (MP Biomedicals, Santa Ana, CA, USA) with 0.2 mL of zirconia-
710 silica beads (BioSpec Products, Bartlesville, OK, USA). Total RNA was then purified with
711 the miRNeasy Mini Kit (Qiagen, Hilden, Germany)[59]. The isolated RNA was treated with
712 DNase and subsequently employ ed for cDNA synthesis with the Maxima H Minus cDNA

713 Synthesis Master Mix (ThermoFisher, Waltham, MA, USA). Real-time PCR was
714 performed with PowerUp SYBR Green Master Mix (ThermoFisher) on a QuantStudio 3
715 qPCR system (ThermoFisher) in triplicate. The primers for qPCR are listed in **Table S2**.
716 Gene expression was normalized to *actA*, relative fold expression was calculated using
717 $2^{-\Delta\Delta Ct}$ method.
718

719 **Small RNA (sRNA) sequencing**

720 sRNA libraries were constructed with the QIAseq miRNA Library Kit (Qiagen) and
721 sequenced on an NovaSeq X platform (Illumina) by 75-bp single end. Raw reads were
722 trimmed with adaptor sequence (5′-GTTCAGAGTTCTACAGTCCGACGATC-3′ and 5′-
723 AACTGTAGGCACCATCAA-3′) utilizing BBDuk. Filtered reads were then mapped to the
724 reference genomes (*M. bainieri* CBS293.63 or *M. atramentarius* CBS202.28) using
725 BBMap[53]. The resulting SAM files were converted to BAM files, and antisense reads were
726 sorted using SAMtools (v1.21)[54]. BAM files were converted to TDF files using IGV tools
727 with a window size of 20 bp and the mean window function. The data was subsequently
728 visualized in the Integrative Genome Viewer (IGV v2.16.0)[60]. The Y-axis reflects the
729 average read coverage per 20 bp window. Peak calling was performed with MACS3 using
730 a fold-enrichment range between 5 and 50. sRNA-seq experiments were performed with
731 one biological sample per strain.
732

733 **Western blot**

734 Each *Mucor* strain was cultivated in YPD, with or without FK506, at room
735 temperature for three days. After overnight lyophilization, each sample was homogenized

736 using a FastPrep bead-beater (MP Biomedicals) with 0.2 mL of zirconia-silica beads
737 (BioSpec Products). Pierce RIPA buffer (ThermoFisher) containing a protease inhibitor
738 tablet (Roche) was then added, and each sample was further disrupted with a FastPrep
739 bead-beater. The samples were incubated on ice for at least 30 min. Cell extracts were
740 centrifuged at 14,000 RPM, 4°C for 10 min, and the supernatants were quantified with
741 the Pierce BCA Protein Assay Kit (ThermoFisher). Next, 20 µg of each sample was mixed
742 with Novex Tris-Glycine SDS Sample Buffer (Invitrogen, Waltham, MA, USA) and boiled
743 at 85°C for 5 min. After briefly cooling, the samples were separated by SDS-PAGE,
744 transferred to a PVDF membrane, and incubated overnight at 4°C with an anti-FKBP12
745 antibody (Invitrogen) or an anti-GAPDH antibody (Proteintech, Rosemont, IL, USA).
746 Following incubation with a horseradish peroxidase-conjugated anti-rabbit antibody,
747 FKBP12 and GAPDH expression were detected on a ChemiDoc MP imaging system (Bio-
748 Rad, Hercules, CA, USA).
749
750 **Chromatin immunoprecipitation (ChIP)-qPCR**
751 A total of 10^6 spores from each *Mucor* strain were inoculated in liquid YPD medium
752 with or without FK506 and incubated overnight at 25°C. The samples were then cross-
753 linked with 1% formaldehyde (ThermoFisher), followed by addition of glycine (Sigma-
754 Aldrich, St. Louis, MO, USA) at a final concentration of 0.125M. After washing and
755 freezing using liquid nitrogen, each sample was ground with a pestle and suspended in
756 ChIP lysis buffer (50 mM HEPES, pH=7.5, 150 mM NaCl, 1 mM EDTA, pH=8, 1% Triton
757 X-100, and 0.1% sodium deoxycholate) containing a protease inhibitor tablet (Roche).

758 Disrupted cells were then sonicated with a Bioruptor (Diagenode) for 40 cycles, with 30s
759 on and 30s off and clarified by centrifuge for 5 min. The input samples were stored at
760 -80°C, while the IP samples were incubated overnight at 4°C with Dynabeads Protein A/G
761 (Invitrogen) pre-conjugated with the anti-histone H3K9 dimethyl antibody (Abcam,
762 Cambridge, UK) or the anti-RNA polymerase II antibody (Active Motif, Carlsbad, CA).
763 Crosslinking between protein and DNA in both input and IP samples was reversed with
764 the MAGnify Chromatin Immunoprecipitation System (Invitrogen), and DNA quality was
765 analyzed using a Qubit (ThermoFisher). qPCR was performed in triplicate with primers
766 described in **Table S2**. H3K9 methylation enrichment was calculated by normalizing the
767 IP DNA to the input DNA with the ΔCt method and further adjusted to the *actA* gene with
768 the ΔΔCt method, followed by $2^{-\Delta\Delta Ct}$ to determine relative enrichment[61,62]. RNA
769 polymerase II enrichment was similarly calculated by normalizing the IP DNA to the input
770 DNA (ΔCt), followed by normalization to an intronic region enriched for siRNAs and
771 marked by H3K9me2 (ΔΔCt). Relative enrichment was determined with the $2^{-\Delta\Delta Ct}$ method.
772

773 **ChIP sequencing**

774 Input and IP libraries were constructed with KAPA HyperPrep (Roche) and
775 sequenced on a NovaSeq X platform (Illumina) by 150-bp paired end. Raw FASTA files
776 were trimmed with Trimmomatic (v0.39) and filtered reads were mapped to the reference
777 genomes (*M. bainieri* CBS293.63 or *M. atramentarius* CBS202.28) using Bowtie2 (v2.5.4)
778 [55,56]. The resulting SAM files were converted to BAM files using SAMtools (v1.21)[54]. Broad
779 ChIP-peak calling was analyzed with MACS3 (v3.0.3) with the parameters --mfold 10
780 1000 and --extsize 147, and enrichment was analyzed by generating coverage files with

781 BamCoverage (v3.5.6), followed by counts per million (CPM) normalization[57,58].
782 Processed BAM files were converted to TDF files IGV tools with a window size of 20 bp
783 and the mean window function and subsequently visualized with IGV (v2.16.0) [63]. ChIP-
784 seq experiments were performed with one biological sample per strain.
785
786 ***In vivo* infection**
787 Six-week-old male BALB/cAnNCrl mice were analyzed in this study. Five mice
788 were infected with each *Mucor* strain. Two days prior to infection, 200 mg/kg of
789 cyclophosphamide (Sigma-Aldrich), an immunosuppressant, was administered
790 intraperitoneally. Each mouse was infected with 1×10^6 spores (in 50 μL PBS) via retro-
791 orbital injection after anesthetizing the mice with isoflurane for 2.5 min. After infection, the
792 mice were monitored twice daily and administered cyclophosphamide at 200 mg/kg body
793 weight every four days. To assess pathogenicity, weight loss was monitored, and any
794 animal experiencing ≥ 20% loss of body weight was humanely euthanized.
795
796 **Strains recovered after *in vivo* passage**
797 To assess fungal burden and isolate *Mucor* strains from organs, five mice per
798 *Mucor* strain were intravenously infected. At the humane endpoint, the brain, lung, liver,
799 and spleen were dissected. Whole organs were homogenized in 0.8 mL of PBS with a
800 bead beater for 2 min, then diluted and plated on YPD supplemented with 50 μg/mL
801 chloramphenicol. After a two-day incubation at room temperature, fungal colonies were
802 picked and patched onto YPD plates with or without FK506 to assess the stability of
803 FK506 resistance following *in vivo* passage. The stability rate was determined by

804 calculating the proportion of resistant colonies on YPD supplemented with FK506 relative
805 to the total colonies patched on YPD[32].
806
807 **QUANTIFICATION AND STATISTICAL ANALYSES**
808 Statistical differences between the control and target strains were evaluated using
809 ordinary one-way ANOVA using Tukey's Honestly Significant Difference (HSD) test with
810 using GraphPad Prism (v10.1.1). Kaplan-Meier survival curves were generated and
811 analyzed with the log-rank test in R (v4.3.2) to estimate survival probability. Data are
812 reported as mean ± standard deviation. In all graphs, p values or asterisks were listed
813 indicating statistical significance ($^{*}p < 0.05$; $^{**}p < 0.01$; $^{***}p < 0.001$; $^{****}p < 0.0001$).

814 **Figure legends**

815 **Figure 1. FK506-resistant strains isolated from the *Mucor circinelloides* complex.**

816 (A) Schematic representation of the procedure followed to obtain FK506- and/or
817 rapamycin-resistant strains from *Mucor circinelloides* complex species. This figure was
818 generated with BioRender.com.

819 (B) Phenotypic analysis of FK506-resistant isolates in *M. janssenii* CBS185.68 (PS1), *M.*
820 *bainieri* CBS293.63 (PS3), and *M. atramentarius* CBS202.28 (PS6).

821 WT, wild-type; M, Mendelian mutant; E, Epimutant.

822

823 **Figure 2. FK506-resistant epimutants exhibit silencing of *fkbA* mRNA and FKBP12**
824 **protein expression and are unstable.**

825 (A, D) Phenotypic reversion of FK506-resistant epimutant strains following serial passage
826 without drug selection in *M. bainieri* (A) or *M. atramentarius* (D). Red arrows indicate the
827 points at which epimutants reverted to the WT phenotype. FK506 was utilized at 1 µg/mL
828 and rapamycin at 100 ng/mL. WT, wild-type; P, number of passages.

829 (B, E) Quantification of the *fkbA* mRNA expression in *M. bainieri* (B) *or M. atramentarius*
830 (E). Error bars represent mean ± SEM (n = 3). Statistical significance: $^{****}p \leq 0.0001$.

831 (C, F) Western blot analysis of FKBP12 protein expression in *M. bainieri* (C) or *M.*
832 *atramentarius* (F).

833 PS3: E1–E9, epimutants; E1P4–E9P24, revertants. PS6: E1 and E2, epimutants; E1P32
834 and E2P28, revertants.

835 **Figure 3. Small RNAs mediate FK506 resistance in *M. bainieri*.**

836 (A) Antisense small RNA coverage mapped across the *fkbA* gene and its neighboring loci.

837 The peaks shown below represent significant enrichment peaks, validated by MACS3.

838 (B) Small RNA abundance (RPM: reads per million) mapped to the *fkbA* gene.

839 (C) 5′-end nucleotide preference of small RNAs associated with the *fkbA* gene.

840 (D) Size distribution of small RNAs mapped to the *fkbA* gene.

841 WT, wild-type; E1–E9, epimutants; E1P4–E9P24, revertants.

842

843 **Figure 4. Heterochromatin marks underlie epigenetic FK506 resistance in *M.***

844 ***bainieri*.**

845 (A) ChIP-qPCR analysis of H3K9me2 enrichment at the positive control region (an siRNA-

846 enriched locus) and *fkbA* locus (targeting the 5′-UTR, exonic regions, and 3′-UTR). Error

847 bars represent mean ± SEM (n = 3). Statistical significance: $^{*}p \leq 0.05$, $^{**}p \leq 0.01$; $^{****}p \leq$

848 0.0001.

849 (B, C) ChIP-seq coverage mapped across the positive control loci (B) or *fkbA* and its

850 neighboring loci (C). The peaks shown below represent significant enrichment peaks,

851 validated by MACS3.

852 (D) ChIP-qPCR analysis of RNA polymerase II enrichment at the positive control region

853 (*actA*), *fkbA* locus (targeting the 5′-UTR and exonic region), a *fkbA*-neighboring gene, and

854 negative control region (an siRNA-enriched locus marked by H3K9me2). Statistical

855 significance: $^{****}p \leq 0.0001$.

856 WT, wild-type; E1–E8, epimutants; E1P4–E8P28, revertants

857 **Figure 5. Heterochromatin-associated FK506 resistance is conserved in *M.***
858 ***atramentarius*.**
859 (A) Antisense small RNA coverage mapped across the *fkbA* gene and its neighboring loci.
860 The peaks shown below represent significant enrichment peaks, validated by MACS3.
861 (B) Small RNA abundance (RPM: reads per million) mapped to the *fkbA* gene.
862 (C) 5′-end nucleotide preference of small RNAs associated with the *fkbA* gene.
863 (D) Size distribution of small RNAs mapped to the *fkbA* gene.
864 (E) ChIP-qPCR analysis of H3K9me2 enrichment at the positive control region (an siRNA-
865 enriched locus) and *fkbA* locus (targeting the 5′-UTR, exonic regions, and 3′-UTR). Error
866 bars represent mean ± SEM (n = 3). Statistical significance: $^{****}p \leq 0.0001$.
867 (F, G) ChIP-seq coverage mapped across the positive control loci (F) or *fkbA* and its
868 neighboring loci (G). The peaks shown below represent significant enrichment peaks,
869 validated by MACS3.
870 (H) ChIP-qPCR analysis of RNA polymerase II enrichment at the positive control region
871 (*actA*), *fkbA* locus (targeting the 5′-UTR and exonic region), a *fkbA*-neighboring gene, and
872 negative control region (an siRNA-enriched locus marked by H3K9me2). Statistical
873 significance: $^{****}p \leq 0.0001$.
874 WT, wild-type; E1 and E2, epimutants; E1P32 and E2P28, revertants.
875
876 **Figure 6. Inherited heterochromatin-mediated antifungal resistance persists after**
877 ***in vivo* passage.**
878 (A) Fungal growth of *M. bainieri* and *M. atramentarius* under different temperature
879 conditions. Microscopic images show enlarged sporangia (scale bar = 20 μm).

880 (B) Survival rates of mice infected with *M. atramentarius*. *Mucor circinelloides* and PBS
881 served as positive and negative controls, respectively. The log-rank test revealed a
882 statistically significant difference in survival between groups (*M. atramentarius* vs PBS, p
883 = 0.014).
884 (C) Fungal colonies recovered from four different organs following *in vivo* infection with
885 wild-type (WT), epimutant (E1), and revertant (E1P32) strains. The bar plot (right) shows
886 the percentage of FK506-resistant colonies from each organ after passage.
887 (D) ChIP-qPCR analysis of H3K9me2 enrichment at the *fkbA* locus following *in vivo*
888 passage, targeting two exonic regions. Error bars represent mean ± SEM (n = 3).
889 Statistical significance: ****$p \leq 0.0001$.
890 WT, wild-type; E1R1–E1R3, FK506-resistant epimutants; E1S1, FK506-sensitive
891 epimutant; E1P32, revertant.
892
893 **Figure 7. Schematic overview of epigenetic genetic silencing contributing to**
894 **antifungal resistance in *Mucor* species.**
895 *fkbA* expression enables FKBP12 production and FK506 sensitivity (yeast-like
896 morphology). Epigenetic silencing of *fkbA* via RNAi or heterochromatin leads to FK506
897 resistance and hyphal growth. Generated with BioRender.com.

898 **Table 1. FK506 resistant strains isolated in this study.**

Species	Name	Phenotype	*fkbA* mutation	Impact on FKBP12	Calcineurin mutation
PS1 *Mucor janssenii*	M1	FK506-R, Rapa-S	No	No	G1496C in *cnaA* (G347A missense mutation)
	M2	FK506-R, Rapa-R	4,324 bp insertion (Unknown) at 38 bp upstream *fkbA* ORF	-	-
	M3	FK506-R, Rapa-R	Large deletion	Loss	-
	M4	FK506-R, Rapa-R	Large deletion	Loss	-
	M5	FK506-R, Rapa-R	5,052 bp insertion (RC/Helitron_DNA transposons) at 16 bp upstream *fkbA* ORF	-	-
	M6	FK506-R, Rapa-R	C120 1 bp deletion in exon 2 (Frameshift)	Nonsense mutation	-
	M7	FK506-R, Rapa-R	Large deletion	Loss	-
	M8	FK506-R, Rapa-R	G258C in 5' splice site of intron2	-	-
	M9	FK506-R, Rapa-R	Large deletion	Loss	-
	M10	FK506-R, Rapa-R	G258C in 5' splice site of intron2	-	-
PS3 *Mucor bainieri*	E1	FK506-R, Rapa-R	No	No	No
	E2	FK506-R, Rapa-R	No	No	No
	E3	FK506-R, Rapa-R	No	No	No
	E4	FK506-R, Rapa-R	No	No	No
	E5	FK506-R, Rapa-R	No	No	No
	E6	FK506-R, Rapa-R	No	No	No
	M1	FK506-R, Rapa-R	C357 1 bp deletion in exon 3 (Frameshift)	Nonsense mutation	No
	E7	FK506-R, Rapa-R	No	No	No
	E8	FK506-R, Rapa-R	No	No	No
	E9	FK506-R, Rapa-R	No	No	No
PS6 *Mucor atramentarius*	M1	FK506-R, Rapa-R	C404 1 bp deletion in exon 3 (Frameshift)	Nonsense mutation	No
	M2	FK506-R, Rapa-S	No	No	G477T in *cnbR* (V122F missense mutation)
	M3	FK506-R, Rapa-R	G249A in 5′ splice site	No	No
	M4	FK506-R, Rapa-R	G249A in 5′ splice site	No	No
	M5	FK506-R, Rapa-S	G189T in exon 2	Synonymous mutation	No
	M6	FK506-R, Rapa-R	C404 1 bp deletion in exon 3 (Frameshift)	Nonsense mutation	No
	M7	FK506-R, Rapa-R	T2C in exon 1 (start-loss mutation)	Loss	No
	E1	FK506-R, Rapa-R	No	No	No
	E2	FK506-R, Rapa-R	No	No	No
	M8	FK506-R, Rapa-R	C404 1 bp deletion in exon 3 (Frameshift)	Nonsense mutation	No

899

900 **Table 2. Epimutant reverted strains analyzed in this study.**

Species	Name	Background	Phenotype	Description
PS3 *Mucor bainieri*	E1P4	E1	FK506-S, Rapa-S	E1 Revertant after passage 4
	E2P4	E2	FK506-S, Rapa-S	E2 Revertant after passage 4
	E3P12	E3	FK506-S, Rapa-S	E3 Revertant after passage 12
	E3P16	E4	FK506-S, Rapa-S	E4 Revertant after passage 16
	E5P12	E5	FK506-S, Rapa-S	E5 Revertant after passage 12
	E6P12	E6	FK506-S, Rapa-S	E6 Revertant after passage 12
	E7P28	E7	FK506-S, Rapa-S	E7 Revertant after passage 28
	E8P28	E8	FK506-S, Rapa-S	E8 Revertant after passage 28
	E9P24	E9	FK506-S, Rapa-S	E9 Revertant after passage 24
PS6 *Mucor atramentarius*	E1P32	E1	FK506-S, Rapa-S	E1 Revertant after passage 32
	E2P28	E2	FK506-S, Rapa-S	E2 Revertant after passage 28

901

902 **Table 3. Summary of epigenetic mechanisms in *Mucor bainieri*.**

Group	Mechanisms	Epimutant	Revertant	Average passages for revertant
1	RNAi-associated heterochromatin-dependent silencing	E1	E1P4	6.67
		E2	E2P4	
		E3	E3P12	
2	Heterochromatin-dependent silencing	E4	E3P16	16
3	Canonical RNAi-dependent silencing	E5	E5P12	18.8
		E6	E6P12	
		E7	E7P28	
		E8	E8P28	
		E9	E9P24	

903

Figure 1. Son et al.

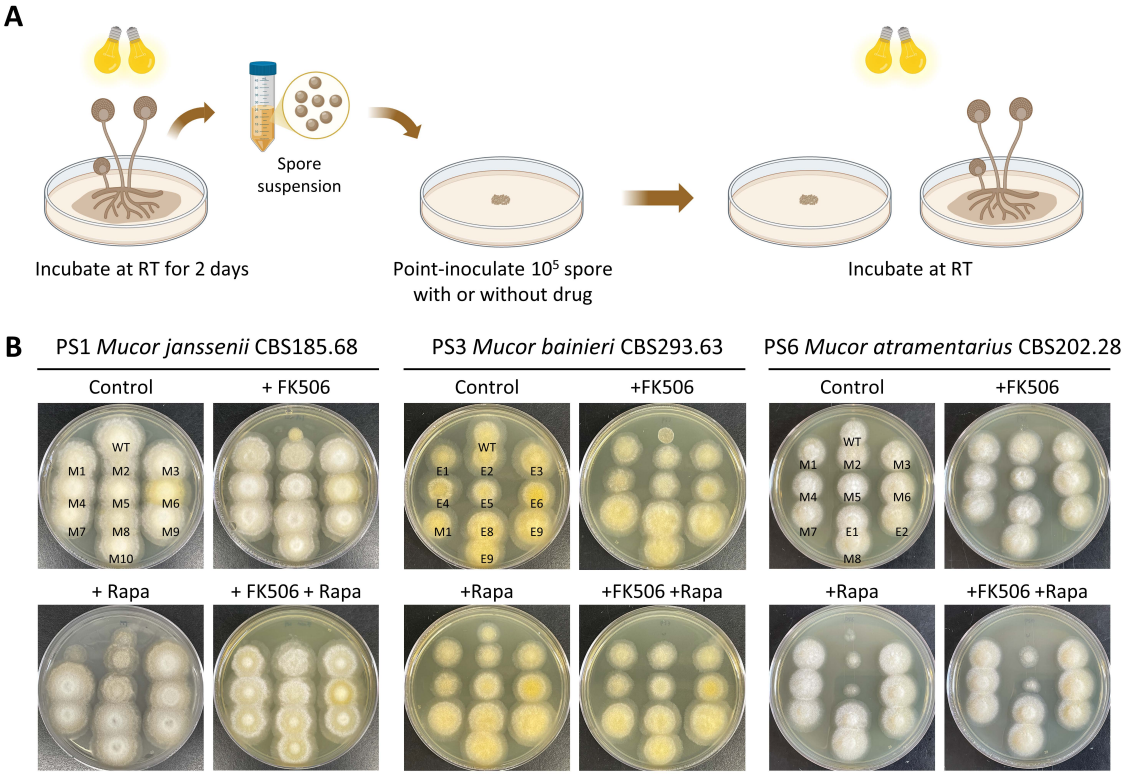

Figure 2. Son et al.

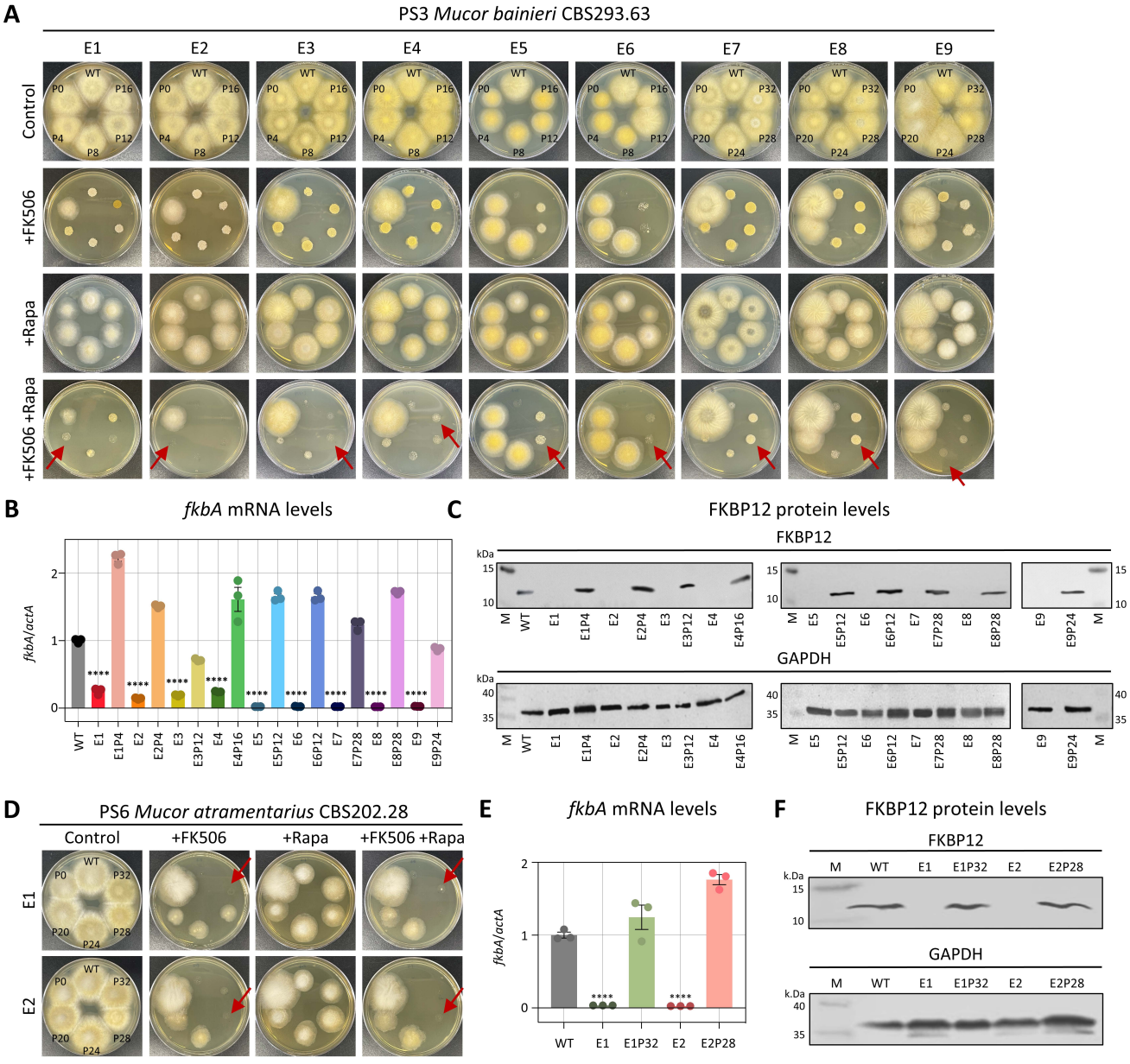

Figure 3. Son et al.

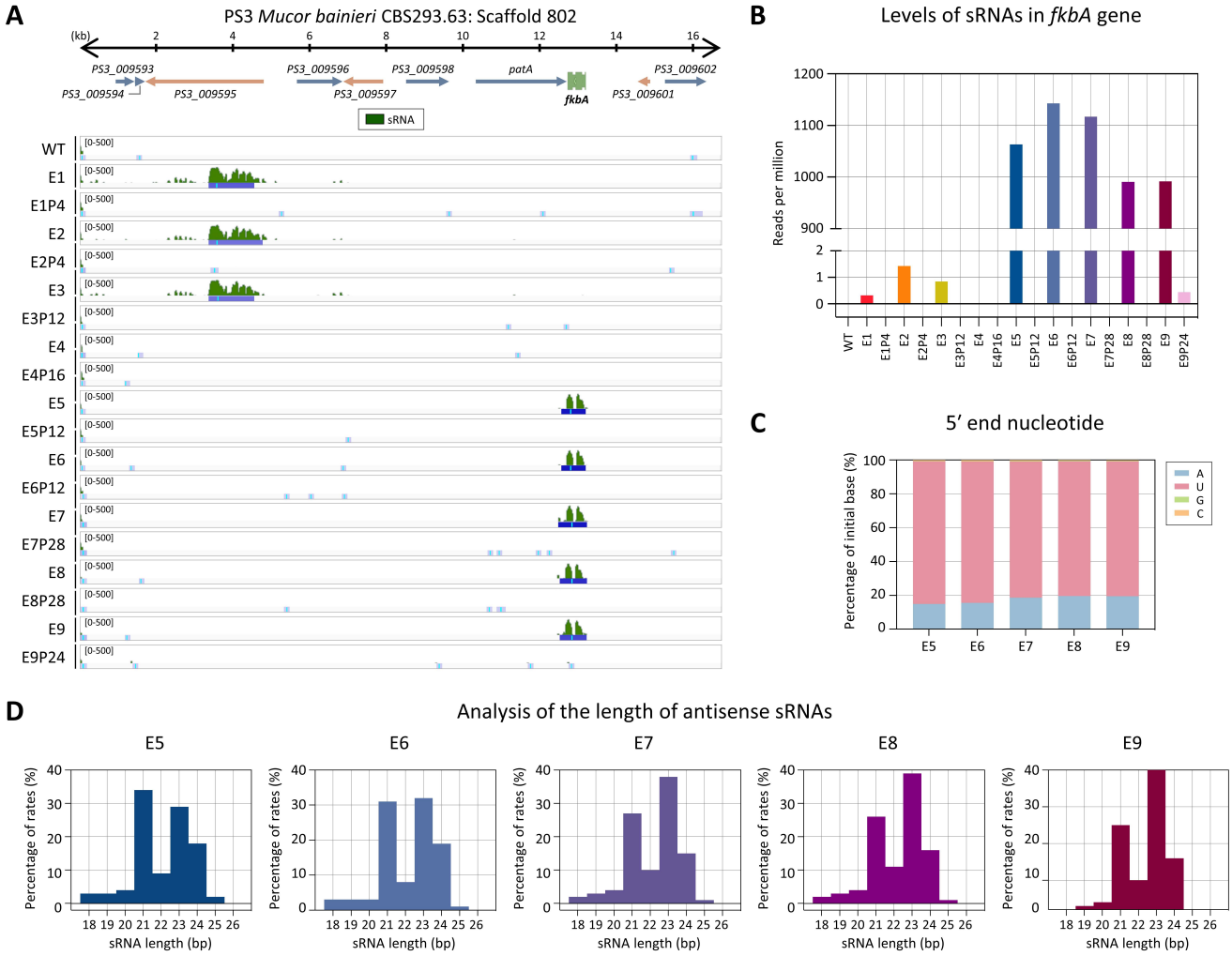

Figure 4. Son et al.

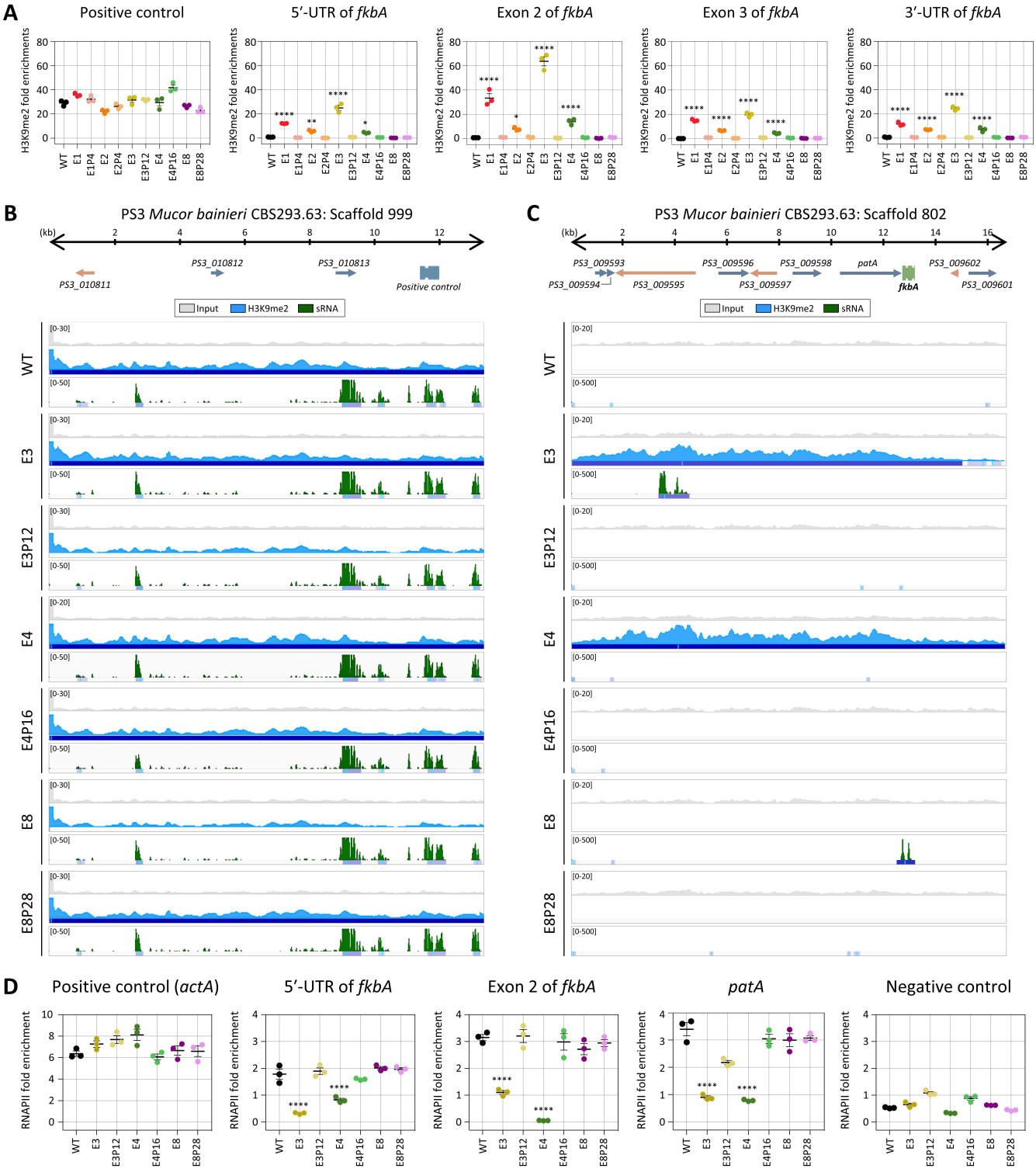

Figure 5. Son et al.

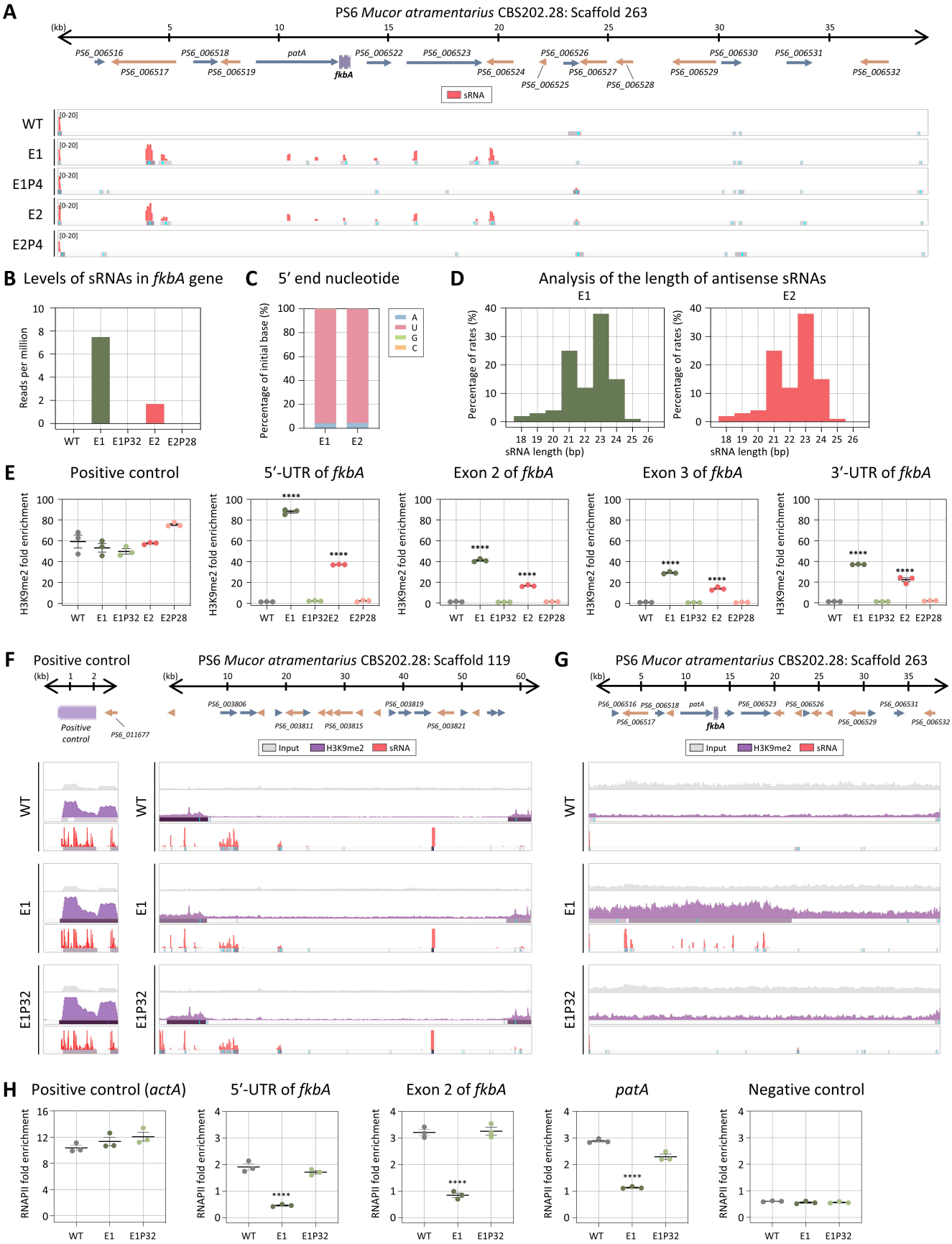

Figure 6. Son et al.

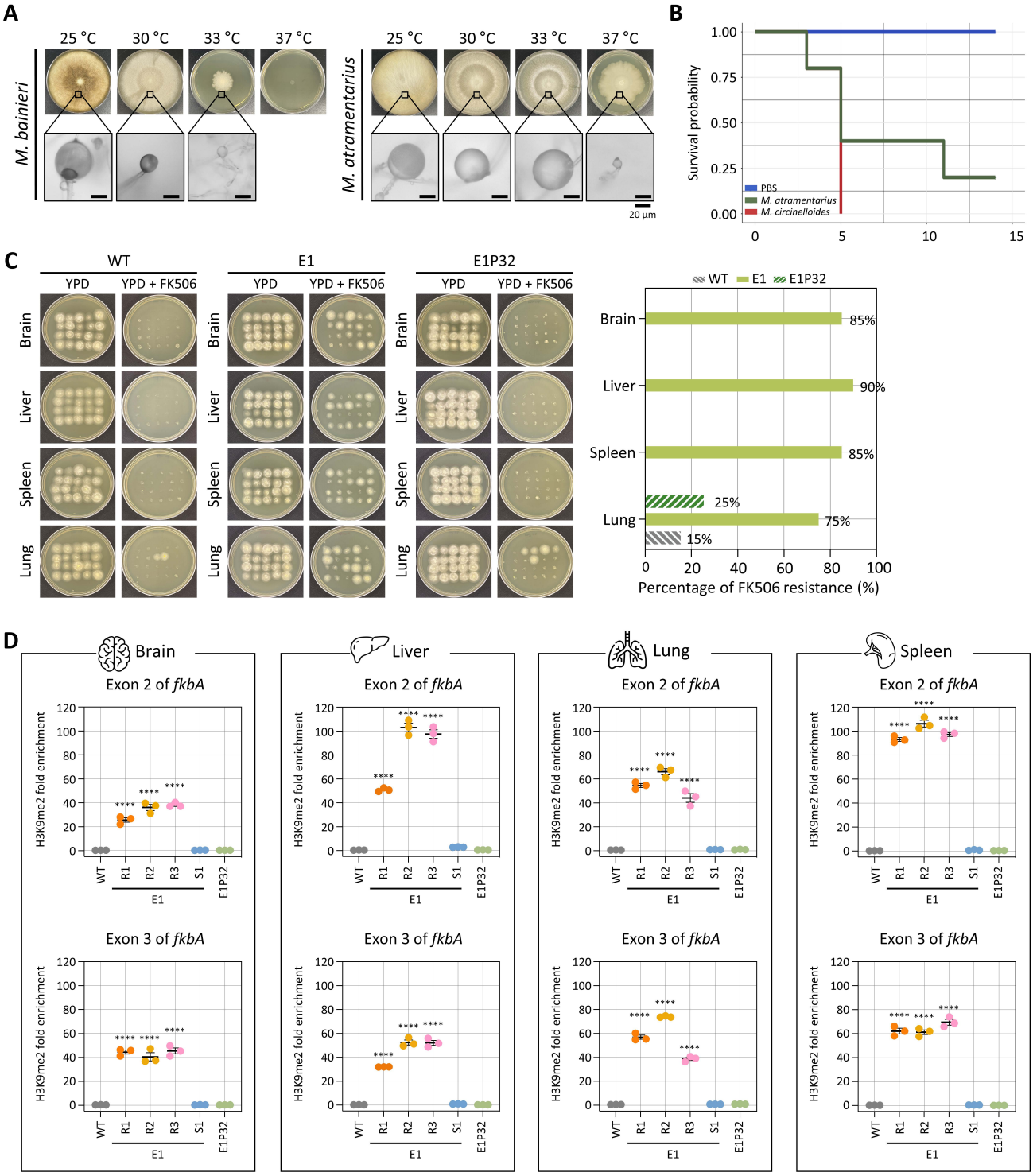
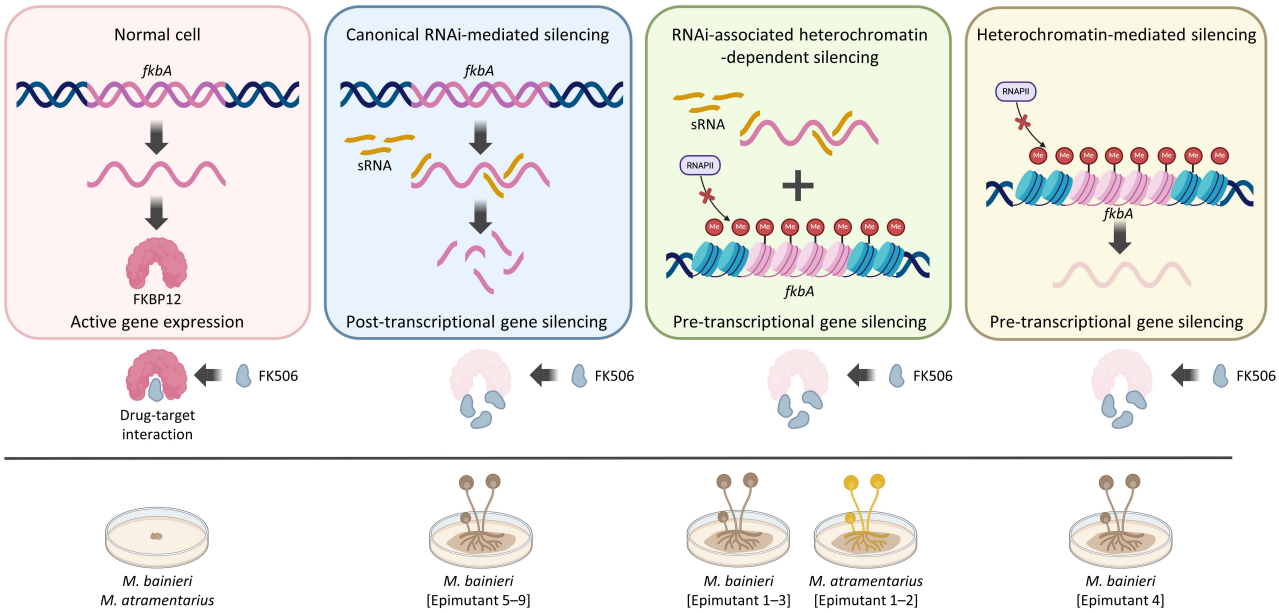
Figure 7. Son et al.